

A WELL-LOG REGRESSION ANALYSIS FOR P-WAVE VELOCITY PREDICTION IN THE NAMORADO OIL FIELD, CAMPOS BASIN

Fabrcio de Oliveira Alves Augusto and Jorge Leonardo Martins

Recebido em 13 abril, 2009 / Aceito em 19 janeiro, 2010
Received on April 13, 2009 / Accepted on January 19, 2010

ABSTRACT. Geophysical well log measurements are key information for the development of oil and gas reservoirs. However, the absence of a certain fundamental well log, for instance, the compressional-wave (P-wave) sonic log, prevents the application of specific risk-assessment techniques. Therefore, the application of methodologies for estimating log records absent in wells is of great importance in the reservoir characterization and development procedures. In this paper, we use the regression analysis methodology for estimating P-wave sonic log measurements. Effective porosity, shaliness and electrical resistivity are established, individually or in a combined way, as the parameters for describing P-wave velocity variation in Namorado oil field, Campos basin. Two general equations provide 28 empirical models with potential use in estimating P-wave velocity variation from well log measurements. Application of least-squares technique leads to the determination of lithology-related regression coefficients at the surroundings of two wells chosen for verifying the empirical models. The results show the equivalence of both general equations used for obtaining empirical models for P-wave velocity estimation. As confirmation of papers published previously, empirical models assuming effective porosity and/or shaliness as dependence parameters play a fundamental role in the prediction of velocity variation. Nevertheless, the velocity calibration process exhibits high stability for empirical models in which electrical resistivity is used as an additional dependence parameter.

Keywords: geophysical well logs, regression analysis, P-wave velocity estimation, Namorado reservoir.

RESUMO. Registros de perfilagem geofísica de poços são informações cruciais para o desenvolvimento de reservatórios de petróleo e gás. Entretanto, a ausência de qualquer perfil geofísico fundamental, por exemplo, o perfil sônico de ondas compressoriais (ondas P), impede a aplicação de técnicas específicas de avaliação de risco. Portanto, a aplicação de metodologias para estimativa de registros de perfis ausentes em poços é de grande importância nos procedimentos de caracterização e desenvolvimento de reservatórios. Neste artigo, usamos a metodologia de análise de regressão para estimar registros de perfil sônico de ondas P. Porosidade efetiva, argilosidade e resistividade elétrica são estabelecidos, individualmente ou de forma combinada, como os parâmetros para descrever a variação da velocidade de ondas P no campo de Namorado, bacia de Campos. Duas equações gerais fornecem 28 modelos empíricos com uso potencial na estimativa da variação de velocidade de ondas P a partir de registros de perfis de poços. A aplicação da técnica de mínimos quadrados conduz à determinação dos coeficientes das regressões relacionados à litologia nas imediações de dois poços escolhidos para verificar os modelos empíricos. Os resultados mostram a equivalência de ambas equações gerais usadas na obtenção dos modelos empíricos para estimativa de velocidade de ondas P. Como confirmação de artigos publicados anteriormente, modelos empíricos que assumem porosidade efetiva e/ou argilosidade como parâmetros da dependência desempenham papel fundamental na descrição da variação da velocidade. Entretanto, o processo de calibração da velocidade exibe alta estabilidade para modelos empíricos nos quais a resistividade elétrica é utilizada como um parâmetro adicional da dependência.

Palavras-chave: perfis geofísicos de poços, análise de regressão, estimativa de velocidade de ondas P, reservatório Namorado.

INTRODUCTION

The geophysical development of an oil and gas field relies on characterizing the variation of petrophysical properties throughout the sedimentary interval containing the reservoirs (Archie, 1950). In this way, laboratory measurements on core plugs, interpretation of geophysical well logs and inversion of seismic attributes provide valuable estimates of reservoir physical properties. Integration of these distinct methodologies is the best approach to determine uncertainties in the predictions, with direct implications on risk mitigation in drilling operations (Pennington, 2001).

The estimation of any physical rock property implies to adopt a mathematical model. However, the selected model hardly contains the full set of parameters affecting the rock property under study. In general, the dependence of a given rock property is studied considering a parameter separately or combining relevant parameters in order to establish a corresponding mathematical model. For instance, let us take the effective-medium theory model routinely used in estimating total porosity from bulk density logs (Dewan, 1983; Ellis, 1987). The model establishes dependence of bulk density of a porous rock on mineralogy, porosity and fluid saturation. Nevertheless, depth and/or effective pressure are parameters ignored in the formulation of the effective-theory model for bulk density. The degree of rock consolidation tends to increase with depth due to effective pressure. As a result of ignoring those parameters in the formulation, the estimate of total porosity using the bulk density model becomes simple. However, no correlation of the density model with the rock consolidation degree and effective pressure is allowed. A further example is the estimation of rock elastic properties (i.e., seismic velocities), which have parameter dependence yet more complex (Wyllie et al., 1956; Wyllie et al., 1958; Klimentos, 1991; Xu & White, 1995). In this case, the Voigt-Reuss and Hashin-Shtrikman effective medium theories (Watt et al., 1976) can be used for estimating the elastic properties of mixed lithologies. However, calculations require detailed description on rock mineralogic constituents and fluid content. Such a description demands time and is often unavailable. Alternatively, use of Biot-Gassmann equations (Toksöz et al., 1976; Domenico, 1976) allows calculating seismic velocities for dry or saturated porous rocks at low- and high-frequency ranges. However, the incompressibilities and densities of the rock matrix and fluid, as well as the fractional total porosity, must be *a priori* known for estimating seismic velocities using Biot-Gassmann equations.

Assuming that a detailed description of the rock composition is unavailable, regression analysis methodology is usually the

procedure used in the study of parameter dependence of seismic velocities in mixed lithologies. In this instance, the investigation is highly simplified as long as individual or combined parameters (i.e., porosity, shaliness, fluid saturation, confining pressure, and others) can be considered in the seismic velocity model formulation. Moreover, either ultrasonic measurements in core plugs (Tosaya & Nur, 1982; Han et al., 1986; Eberhart-Phillips et al., 1989) or well log data (Raymer et al., 1980; Castagna et al., 1985; Miller & Stewart, 1990) can be the source of information used in regression analysis for parameter dependence studies of seismic velocities. In this way, interpreters gain insight for linking rock properties to attributes investigated, for instance, in oil-bearing reservoir characterization procedures (Krief et al., 1990; Murphy et al., 1991; Castagna et al., 1993).

From Wyllie's et al. (1956, 1958) time-average equation and Raymer et al. (1980) quadratic approach, rock porosity represents the main parameter affecting P-wave velocities. However, both approximations can hardly predict velocity in shaly sandstones without significant misfits. In order to consider additional parameters into the velocity dependence, a useful strategy is the application of multivariate linear regression methodologies. The papers of Tosaya & Nur (1982), Han et al. (1986) and Miller & Stewart (1990) use rock porosity and shaliness to investigate dependence of seismic velocities on both parameters in distinct mixed lithologies. As a result, including shaliness as a further parameter into the dependence significantly increases correlation with velocity measurements. In turn, Eberhart-Phillips et al. (1989) used Han's et al. (1986) core plug data to show that effective pressure plays a significant role in predicting seismic velocities. As a common conclusion from these cited works, porosity and shaliness play a fundamental role in the variation of seismic velocities.

In this paper we refine the regression analysis methodology used in previous investigations (see Han et al., 1986; Eberhart-Phillips et al., 1989; Miller & Stewart, 1990). We take into account empirical models involving fractional effective porosity, shaliness and additionally electrical resistivity as dependence parameters of P-wave velocity variation. Incorporation of electrical resistivity into empirical models has the purpose of incorporating the effects of fluid saturation on the velocity variation, as studied by Domenico (1974). Two general equations provide 28 multivariate linear and nonlinear empirical models, which served for estimating P-wave velocity variation through the sedimentary interval corresponding to the upper Macaé formation, Campos basin. Approximately 40 vertical wells were drilled through this turbiditic formation (Tigre & Lucchesi, 1986), through which anomalies

in fundamental geophysical well log measurements reveal variations of physical properties in the Namorado oil field. However, the absence of the P-wave sonic log in most wells prevents constructing normal-incidence synthetic seismograms required for seismic calibration procedures. Hence, the establishment of P-wave velocity models allow sonic log estimation by using correspondent wells at the vicinities. Oliveira & Martins (2003) performed similar regression study using well log measurements only from the Namorado sandstone intervals. Here we extended their regression methodology to the whole mixed lithology column representing the upper Macaé formation. The well log regression methodology will be described in the next section.

METHODOLOGY

In the following, we present the steps for investigating the application of 28 empirical relations for predicting P-wave sonic logs. We selected two wells from the so-called data set "Campo Escola Namorado", which is distributed by ANP/Brazil – Agência Nacional do Petróleo, Gás Natural e Biocombustíveis, to Brazilian universities and research institutions for academic purposes. The data set contains geological and geophysical well log information of more than 40 vertical wells drilled through the upper Macaé formation. In this sedimentary interval the rocks correspond mostly to sandstones and shales of turbiditic origin, forming the offshore oil-producing Namorado field in Campos basin (Tigre & Lucchesi, 1986). Fundamental logs, i.e., gamma ray (GR), deep electrical resistivity (ILD), neutron porosity (NPHI) and bulk density (RHOB) describe variation of physical properties through the formation at the surroundings of correspondent wells, allowing identification of the oil-bearing Namorado sandstone reservoir. The well log data set has no information on shear-wave (S-wave) sonic log, while only a limited number of wells have the corresponding P-wave sonic logs. However, at well locations where sonic logs are unavailable, linear and nonlinear empirical models for the variation of P-wave velocity in the upper Macaé formation can be established. Based on information from the literature, we assumed three main dependence parameters: the fractional effective porosity ϕ_e , the fractional shale volume V_{clay} (i.e., shaliness) and the deep electrical resistivity R_{ild} . Conventional processing of bulk density, gamma ray and induction resistivity logs allows estimating the three mentioned dependence parameters. We applied the classical least-squares technique for determining the regression coefficients of each empirical model. Using the correlation coefficient r , we measure the calibration step uncertainty. Below we summarize the steps of the methodology.

Selection of well logs

Figure 1 shows part of the structural map of the Namorado field. The reservoir resembles a mini-horst bounding by normal faults. Circles and squares denote the vertical wells drilled in the area. We selected two wells containing fundamental log measurements, including the P-wave sonic log. It corresponds to a critical information for the regression analysis and, obviously, for the calibration process with the empirical models proposed. In Figure 1, filled squares indicate the selected wells, named as well-4 and well-37. The log measurements at well-4 are shown in Figure 2; the logs at well-37 are exhibited in Figure 3. In both wells, a high radioactive shale marks the top of the upper Macaé formation as shown by the gamma-ray logs. Further inspection of Figure 2 reveals two main oil-bearing, high-porosity sandstones intervals correlating to resistivity and density anomalies. Sealing lithologies are mostly composites of clay and silt, with some occurrence of carbonates. The lower limit of the Macaé formation represents calcilutites, which are easily identified in both wells by observing the abrupt variation in gamma-ray readings around 3120 m.

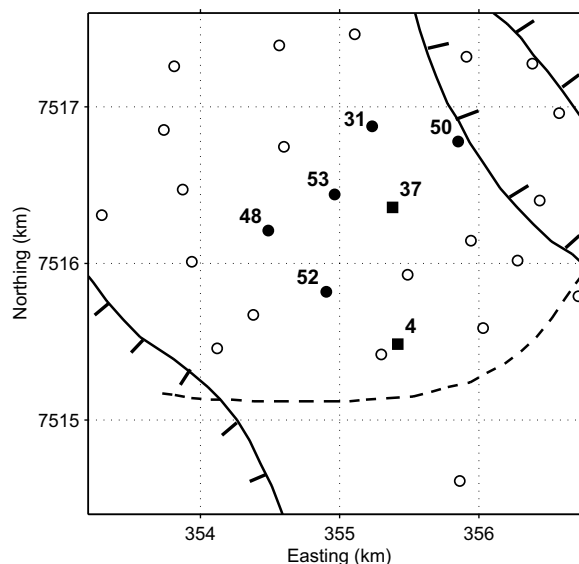


Figure 1 – Partial view of the structural map of Namorado oil field. Full and dashed lines represent the reservoir boundaries. Additional symbols denote well locations: circles "○" correspond to well locations with incomplete and/or absent logs, filled circles "●" are wells with complete logs (excluding the P-wave sonic log), and filled boxes "■" represent wells containing complete logs, including the P-wave sonic log. We refer to "incomplete logs" when the log shows interruptions in the readings.

Shaliness estimation

Well log petrophysics relies on empirical models to estimate rock physical properties. Concerning shaliness V_{clay} estimation, use of gamma-ray measurements is typical in well log interpretation

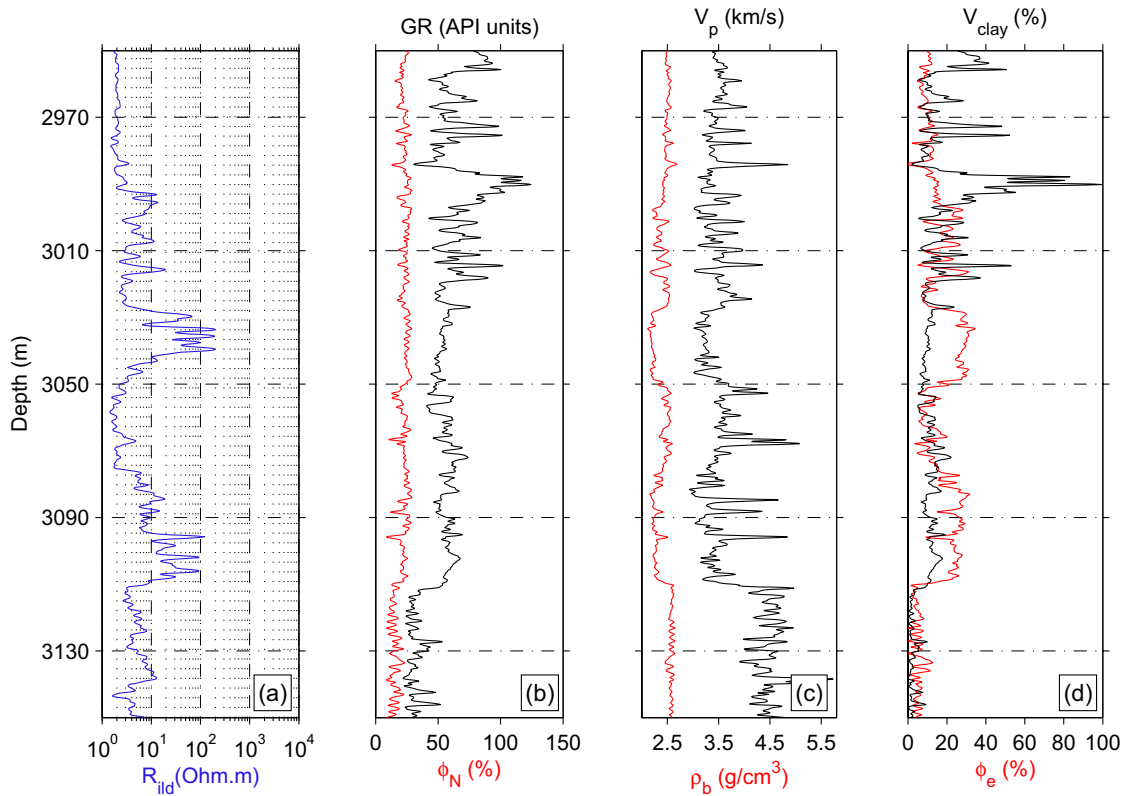


Figure 2 – Geophysical logs at well-4: (a) induction resistivity (ILD, in blue) in Ohm.m; (b) neutron porosity (NPHI, in red) in percentage and gamma-ray GR (API units); (c) bulk density (RHOB, in red) in g/cm³ and the P-wave velocity v_p (km/s) profile converted from the measured sonic log; (d) effective porosity (ϕ_e , in red) and shaliness V_{clay} , both in percentage. Application of Eqs. (1) and (3) allowed estimating V_{clay} and ϕ_e , respectively.

steps. In this case, Larionov (1969) presents empirical formulas for V_{clay} estimation based on sediment consolidation. Taking into account that the Namorado sandstone is from Tertiary age (i.e., the sediments are unconsolidated), we applied Larionov's (1969) equation for shaliness estimation expressed as

$$V_{clay} = 0.083 \left(2^{3.70 \times IGR} - 1 \right). \quad (1)$$

In the preceding equation, the gamma-ray index IGR is given by

$$IGR = \frac{GR_i - GR_{ss}}{GR_{sh} - GR_{ss}}, \quad (2)$$

where GR_i denotes the i^{th} gamma-ray log reading. The quantities GR_{ss} and GR_{sh} are the minimum and maximum readings in the gamma-ray log taken in the sandstone and in the shale point, respectively, in the same formation under study (Dewan, 1983; Ellis, 1987). For the sedimentary interval corresponding to the upper Macaé formation, $GR_{ss} \approx 22$ API units and $GR_{sh} \approx 125$ API units.

Effective porosity estimation

The following formula allows fractional effective porosity ϕ_e estimation from the bulk density log:

$$\phi_e = \phi_t - V_{clay} \frac{\rho_{ma} - \rho_{sh}}{\rho_{ma} - \rho_f}, \quad (3)$$

where ϕ_t is the fractional total porosity

$$\phi_t = \frac{\rho_{ma} - \rho_b}{\rho_{ma} - \rho_f}. \quad (4)$$

The parameter ρ_b represents a reading in the bulk density log. As the upper Macaé formation has quartzose matrix, we take $\rho_{ma} = 2.65$ g/cm³. For the brine formation density, we assume $\rho_f = 1.10$ g/cm³. Dewan (1983) shows that a way of assessing the density at the shale point ρ_{sh} is to take the difference between the density at the shale point and the total porosity log at its maximum, i.e., $\max(\phi_{ni} - \phi_{ti})$, where ϕ_{ni} and ϕ_{ti} correspond to the i^{th} sample of the neutron porosity and the total porosity logs, respectively. In both wells under study the density at the shale point is nearly $\rho_{sh} = 2.66$ g/cm³. Note that in Eq. (3) the shaliness corrects the total porosity yielding the effective porosity ϕ_e .

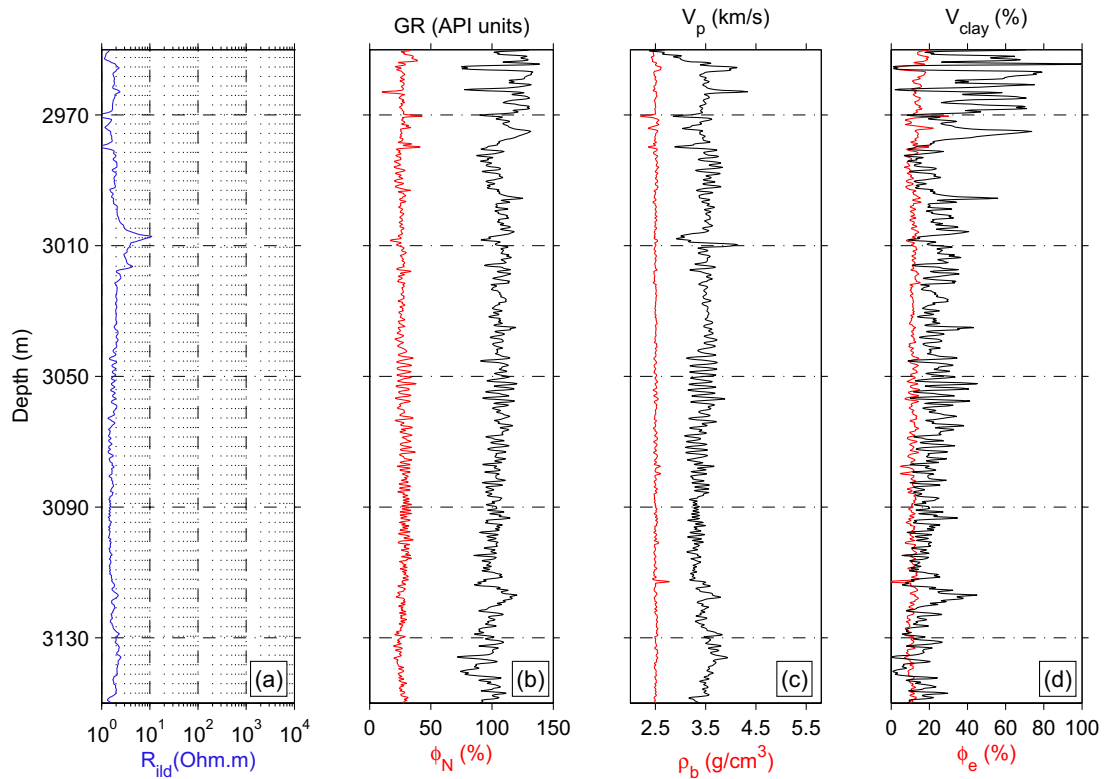


Figure 3 – Geophysical logs at well-37; logs are displayed using the same color code as in Figure 2. Eqs. (1) and (3) were also respectively considered for estimating the variation of shaliness and effective porosity.

Regression analysis

The dependence of P-wave velocity in rocks is attributed to numerous factors. However, in order to simplify the investigation, the evidence in most published papers is the use of empirical models attempting to correlate velocity variation with specific attributes. For example, correlation of velocities with depth and geological time is presented in Faust (1951), while lithology is the parameter of the correlation in Faust (1953). Further empirical models for describing velocity variation based purely on mathematical functions can be found in Kaufman (1953).

In this paper, we assume the general dependence for P-wave velocity model as $v_p = v_p(x, y, z)$, in which the parameters of the dependence are: effective porosity $x \equiv \phi_e$, shaliness $y \equiv V_{clay}$ and electrical resistivity $z \equiv R_{ild}$. The choice of v_p dependence was done taking the physical basis into account, and is corroborated by the results of several papers (see Han et al., 1986; Miller & Stewart, 1990; Oliveira & Martins, 2003). Thus, assuming $x \equiv \phi_e$ and $y \equiv V_{clay}$, we followed the work of previous investigators. Moreover, the incorporation of $z \equiv R_{ild}$ into some empirical models led to the known dependence of P-wave velocity on fluid saturation.

The following general relations allow the investigation of linear and nonlinear empirical models for P-wave velocity prediction from well log measurements:

$$v_p^{mod} = \mathcal{V}_{P0} + \mathcal{V}_{P1} + \mathcal{V}_{P2} + \mathcal{V}_{P3} \tag{5}$$

and

$$v_p^{mod} = \mathcal{V}_{P0} \exp [\mathcal{V}_{P1} + \mathcal{V}_{P2} + \mathcal{V}_{P3}]. \tag{6}$$

The above quantities $\mathcal{V}_{P0}, \mathcal{V}_{P1} \equiv \mathcal{V}_{P1}(x, y, z), \mathcal{V}_{P2} \equiv \mathcal{V}_{P2}(x, y, z)$ and $\mathcal{V}_{P3} \equiv \mathcal{V}_{P3}(x, y, z)$ are written as

$$\mathcal{V}_{P0} \equiv a_0, \tag{7}$$

$$\mathcal{V}_{P1} \equiv a_1 x + a_2 y + a_3 z, \tag{8}$$

$$\mathcal{V}_{P2} \equiv a_4 x y + a_5 x z + a_6 y z, \tag{9}$$

and

$$\mathcal{V}_{P3} \equiv a_7 x^2 + a_8 y^2 + a_9 z^2. \tag{10}$$

We tested the whole set of combinations for empirical formulas possibly provided by Eqs. (5) and (6). These models are easily

obtained by assuming a dependence of v_p on a single parameter, or taking more than one parameter simultaneously in the dependence. For instance, assuming a simple model in which the fractional effective porosity ϕ_e is the only parameter of the dependence, we can write a linear model for P-wave velocity variation

$$v_p^{\text{mod}} = a_0 + a_1 \phi_e. \quad (11)$$

In accordance to Eq. (6), a nonlinear dependence on ϕ_e can also be provided for v_p , as follows

$$v_p^{\text{mod}} = a_0 \exp [a_1 \phi_e]. \quad (12)$$

As in Castagna et al. (1993), we can also use the simple parabolic model with $y \equiv V_{\text{clay}}$ as the only parameter affecting v_p . As a result, we obtain from Eq. (5)

$$v_p^{\text{mod}} = a_0 + a_2 V_{\text{clay}} + a_8 (V_{\text{clay}})^2, \quad (13)$$

On the other hand, Eq. (6) gives a nonlinear empirical model for v_p as a function of V_{clay} :

$$v_p^{\text{mod}} = a_0 \exp [a_2 V_{\text{clay}} + a_8 (V_{\text{clay}})^2]. \quad (14)$$

Besides multivariate linear models as in Han et al. (1986) and in Eberhart-Phillips et al. (1989), Eqs. (5) and (6) also allow to derive nonlinear models. For instance, assuming the parameter dependence $v_p \equiv v_p(\phi_e, V_{\text{clay}}, R_{\text{ild}})$, P-wave velocity can be described by the following multivariate linear model

$$v_p^{\text{mod}} = a_0 + a_1 \phi_e + a_2 V_{\text{clay}} + a_3 R_{\text{ild}}, \quad (15)$$

or, from the general form in Eq. (6), by a multivariate nonlinear model written as

$$v_p^{\text{mod}} = a_0 \exp [a_1 \phi_e + a_2 V_{\text{clay}} + a_3 R_{\text{ild}}]. \quad (16)$$

Two- and three-variable quadratic empirical models can also be derived from Eqs. (5) and (6). Taking $x \equiv \phi_e$ and $z \equiv R_{\text{ild}}$ as the parameters of the dependence, the P-wave velocity variation can be described as

$$v_p^{\text{mod}} = a_0 + a_1 \phi_e + a_3 R_{\text{ild}} + a_5 \phi_e R_{\text{ild}} + a_7 (\phi_e)^2 + a_9 (R_{\text{ild}})^2, \quad (17)$$

and

$$v_p^{\text{mod}} = a_0 \exp [a_1 \phi_e + a_3 R_{\text{ild}} + a_5 \phi_e R_{\text{ild}} + a_7 (\phi_e)^2 + a_9 (R_{\text{ild}})^2]. \quad (18)$$

In summary, we investigated 28 empirical models for predicting P-wave velocities using geophysical well logs. In order to determine the regression coefficients a_i of the corresponding empirical model, we applied the classical least-squares technique (Lines & Treitel, 1984). We thus minimized the square of the residuals between the measured velocity v_p^{meas} (i.e., the readings in the P-wave sonic log) and the modeled velocity v_p^{mod} (i.e., the chosen empirical model). As a result, after constructing the objective function $\mathcal{E}^2 \equiv \mathcal{E}^2(a_i)$

$$\mathcal{E}^2 = |v_p^{\text{meas}} - v_p^{\text{mod}}|^2 \quad (19)$$

we operate $\partial \mathcal{E}^2 / \partial a_i \equiv 0$. The sought coefficients a_i are the unknowns of the resulting linear system of equations derived after minimizing Eq. (19). Notice that we applied the neperian logarithm to both sides of Eq. (6) before operating the derivative of the objective function. Furthermore, we determined the correlation coefficient r in order to investigate the uncertainty in the predictions of P-wave velocities.

Calibration

In the calibration step, we focused on plotting the P-wave velocity logs at both selected wells and the empirical models provided by Eqs. (5) and (6). This procedure aimed at visually inspecting the misfits between measured and predicted v_p velocity logs. Further determination of correlation coefficients of the least-squares regression models and absolute residuals helped analyzing the confidence on the investigated empirical models.

RESULTS

Following the methodology described above, we combined the dependence parameters ϕ_e , V_{clay} and R_{ild} in order to obtain models for v_p velocity variation at both selected wells (see Fig. 1). The least-squares regression coefficients for all 28 empirical models derived from Eqs. (5) and (6) are exhibited in Tables 1-4. Observing the magnitude of the correlation coefficient for corresponding empirical models, we immediately conclude that the general forms in Eqs. (5) and (6) provide equivalent P-wave velocity predictions.

For empirical models with only one variable, it can be observed in the tables that the correlation coefficient reaches the highest magnitude if the effective porosity ϕ_e is chosen for describing v_p dependence. On the other hand, if the parameter of the dependence is the resistivity R_{ild} , the correlation coefficient attains the smallest magnitude. This is indeed an expected result already published in Han et al. (1986), that is, porosity plays a fundamental

Table 1 – Least-squares regression coefficients for P-wave velocity models at well-4. Two general forms are considered: $v_p = a_0 + a_1 x + a_2 y + a_3 z$ and $v_p = a_0 \exp[a_1 x + a_2 y + a_3 z]$. Fractional effective porosity ($x \equiv \phi_e$), shaliness ($y \equiv V_{clay}$) and electrical resistivity ($z \equiv R_{ild}$ in Ohm.m) are the parameters of the dependence shown in the first column of the table. Each column in (a) and (b) provides six empirical models. Between braces are the coefficients associated to exponential empirical models. In order to obtain a velocity model, simply neglect one or two dependence parameters in both considered general forms. The last column in (c) provides the two empirical models having full parameter dependence. Regression coefficients have units in such a way that v_p is in km/s. The symbol r stands for correlation coefficient.

PD	(a)			(b)			(c)
x	ϕ_e			V_{clay}	ϕ_e	ϕ_e	ϕ_e
y		V_{clay}		R_{ild}	R_{ild}	V_{clay}	V_{clay}
z			R_{ild}				R_{ild}
a_0	4.27	3.92	3.72	3.97	4.29	4.42	4.43
a_1	-4.00				-4.40	-3.76	-4.06
a_2		-1.79		-1.84		-1.44	-1.38
a_3			-3.56×10^{-3}	-4.05×10^{-3}	3.30×10^{-3}		2.40×10^{-3}
r	0.70	0.42	0.17	0.47	0.72	0.78	0.79
{ a_0 }	4.26	3.87	3.69	3.93	4.28	4.43	4.44
{ a_1 }	-1.06				-1.15	-9.90×10^{-1}	-1.07
{ a_2 }		-4.60×10^{-1}		-4.70×10^{-1}		-3.60×10^{-1}	-3.50×10^{-1}
{ a_3 }			-9.88×10^{-4}	-1.11×10^{-3}	8.16×10^{-4}		5.87×10^{-4}
{r}	0.71	0.45	0.17	0.49	0.73	0.79	0.80

Table 2 – Least-squares regression coefficients for P-wave velocity models at well-4, but assuming the following general forms: $v_p = a_0 + a_1 x + a_2 y + a_3 z + a_4 xy + a_5 xz + a_6 yz + a_7 x^2 + a_8 y^2 + a_9 z^2$ and $v_p = a_0 \exp[a_1 x + a_2 y + a_3 z + a_4 xy + a_5 xz + a_6 yz + a_7 x^2 + a_8 y^2 + a_9 z^2]$. The same observations in Table 1 concerning empirical model derivation, parameter dependence and units apply for Table 2.

PD	(a)			(b)			(c)
x	ϕ_e			V_{clay}	ϕ_e	ϕ_e	ϕ_e
y		V_{clay}		R_{ild}	R_{ild}	V_{clay}	V_{clay}
z			R_{ild}				R_{ild}
a_0	4.74	4.20	3.75	4.29	4.67	4.80	4.71
a_1	-12.15				-12.59	-8.20	-8.23
a_2		-5.50		-5.65		-4.32	-3.91
a_3			-7.51×10^{-3}	-1.22×10^{-2}	2.59×10^{-2}		2.14×10^{-2}
a_4						12.72	8.99
a_5					-8.24×10^{-2}		-5.35×10^{-2}
a_6				3.87×10^{-2}			-1.18×10^{-3}
a_7	24.82				26.90	10.43	11.45
a_8		6.26		6.18		2.58	2.85
a_9			2.69×10^{-5}	3.06×10^{-5}	-1.77×10^{-5}		-3.18×10^{-5}
r	0.74	0.59	0.19	0.62	0.81	0.83	0.85
{ a_0 }	4.76	4.17	3.72	4.27	4.68	4.83	4.72
{ a_1 }	-2.99				-3.09	-1.95	-1.94
{ a_2 }		-1.39		-1.45		-1.07	-9.71×10^{-1}
{ a_3 }			-2.10×10^{-3}	-3.64×10^{-3}	6.45×10^{-3}		5.31×10^{-3}
{ a_4 }						2.94	1.99
{ a_5 }					-1.99×10^{-2}		-1.26×10^{-2}
{ a_6 }				1.25×10^{-2}			-2.32×10^{-4}
{ a_7 }	5.89				6.35	2.21	2.37
{ a_8 }		1.58		1.56		6.48×10^{-1}	7.28×10^{-1}
{ a_9 }			7.63×10^{-6}	8.90×10^{-6}	-3.71×10^{-6}		-8.85×10^{-6}
{r}	0.78	0.61	0.19	0.64	0.81	0.84	0.85

Table 3 – Least-squares regression coefficients for P-wave velocity models at well-37. Two general forms are considered: $v_p = a_0 + a_1 x + a_2 y + a_3 z$ and $v_p = a_0 \exp[a_1 x + a_2 y + a_3 z]$. The same observations in Table 1 concerning empirical model derivation, parameter dependence and units apply for Table 3.

PD	(a)			(b)			(c)
x	ϕ_e				ϕ_e	ϕ_e	ϕ_e
y		V_{clay}		V_{clay}		V_{clay}	V_{clay}
z			R_{ild}	R_{ild}	R_{ild}		R_{ild}
a_0	3.88	3.49	3.40	3.44	3.84	3.94	3.90
a_1	-3.81				-3.76	-5.11	-5.07
a_2		-1.67×10^{-1}		-1.58×10^{-1}		3.88×10^{-1}	3.89×10^{-1}
a_3			2.66×10^{-2}	2.53×10^{-2}	1.85×10^{-2}		1.88×10^{-2}
r	0.46	0.11	0.11	0.16	0.47	0.50	0.51
{ a_0 }	3.92	3.48	3.39	3.43	3.88	3.99	3.95
{ a_1 }	-1.14				-1.13	-1.53	-1.52
{ a_2 }		-4.93×10^{-2}		-4.71×10^{-2}		1.17×10^{-1}	1.17×10^{-1}
{ a_3 }			7.30×10^{-3}	6.92×10^{-3}	4.86×10^{-3}		4.96×10^{-3}
{r}	0.46	0.11	0.11	0.15	0.47	0.50	0.51

Table 4 – Least-squares regression coefficients for P-wave velocity models at well-37, but assuming the following general forms: $v_p = a_0 + a_1 x + a_2 y + a_3 z + a_4 xy + a_5 xz + a_6 yz + a_7 x^2 + a_8 y^2 + a_9 z^2$ and $v_p = a_0 \exp[a_1 x + a_2 y + a_3 z + a_4 xy + a_5 xz + a_6 yz + a_7 x^2 + a_8 y^2 + a_9 z^2]$. The same observations in Table 1 concerning empirical model derivation, parameter dependence and units apply for Table 4.

PD	(a)			(b)			(c)
x	ϕ_e				ϕ_e	ϕ_e	ϕ_e
y		V_{clay}		V_{clay}		V_{clay}	V_{clay}
z			R_{ild}	R_{ild}	R_{ild}		R_{ild}
a_0	3.84	3.53	2.92	2.93	3.53	3.86	3.80
a_1	-3.07				-5.39	-4.22	-4.31
a_2		-4.91×10^{-1}		-2.81×10^{-1}		7.15×10^{-1}	5.52×10^{-1}
a_3			3.61×10^{-1}	4.11×10^{-1}	2.56×10^{-1}		6.93×10^{-2}
a_4						-5.58	3.10
a_5					5.26×10^{-1}		-6.16×10^{-1}
a_6				-1.58×10^{-1}			9.14×10^{-3}
a_7	-2.95				5.60	1.14	-2.40
a_8		4.52×10^{-1}		5.70×10^{-1}		6.37×10^{-1}	-8.10×10^{-1}
a_9			-3.86×10^{-2}	-4.08×10^{-2}	-3.44×10^{-2}		2.27×10^{-3}
r	0.46	0.13	0.53	0.56	0.65	0.51	0.47
{ a_0 }	3.83	3.52	2.95	2.97	3.55	3.85	3.84
{ a_1 }	-7.59×10^{-1}				-1.57	-1.09	-1.26
{ a_2 }		-1.37×10^{-1}		-9.43×10^{-2}		2.37×10^{-1}	1.85×10^{-1}
{ a_3 }			1.06×10^{-1}	1.18×10^{-1}	6.90×10^{-2}		1.41×10^{-2}
{ a_4 }						-1.92	7.63×10^{-1}
{ a_5 }					2.02×10^{-1}		-1.37×10^{-1}
{ a_6 }				-3.76×10^{-2}			2.70×10^{-3}
{ a_7 }	-1.52				1.78	-1.28×10^{-1}	-1.04
{ a_8 }		1.22×10^{-1}		1.61×10^{-1}		2.08×10^{-1}	-2.39×10^{-1}
{ a_9 }			-1.14×10^{-2}	-1.20×10^{-2}	-1.01×10^{-2}		7.03×10^{-4}
{r}	0.46	0.13	0.54	0.56	0.66	0.51	0.47

role in the variation of P-wave velocity, while the influence of shaliness V_{clay} is smaller than ϕ_e . The assumption of resistivity as a parameter of influence in the v_p variation represents an attempt of considering fluid saturation. However, the resistivity R_{ild} exerts the smallest influence on v_p variation. Note that the results in the third column of Table 4a represent an exception. We interpret these results as the footprint of the well-behaved resistivity and porosity logs at well-37. At this well, it seems that fluid content predominantly influences the velocities. A further interesting result can be obtained as follows. Let us consider all 2-variable empirical models in which ϕ_e and V_{clay} are the governing parameters in the v_p variation. If we assume ϕ_e and V_{clay} as null quantities in these velocity models, the maximum P-wave velocity for the considered quartzose matrix will hardly be $v_p = 4.90$ km/s as seen in the third column of item (b) of all tables. Taking into account that $v_p = 5.94$ km/s is the velocity value recommended for quartz (Wyllie et al., 1958), the latter result for $V_{\text{clay}} = 0.0$

clearly indicates the influence of other different lithologies (i.e., carbonates) present in the formation. Actually, this analysis can be applied for all empirical models used in this investigation. The velocity calibration using the above-mentioned empirical models is presented in the Figures 4 and 6, including the corresponding equivalent models obtained from Eq. (6).

In Tables 2a and 4a, the magnitude of the correlation coefficients shows that use of quadratic regression models improves the confidence on P-wave velocity predictions. The plots in Figures 5 and 7 exhibits velocity calibration for both wells under investigation, confirming the high performance of all quadratic models used. In summary, incorporation of quadratic terms into the empirical models decreases the misfits between measured and predicted velocities. As pointed out above, the small-magnitude discrepancies between measured and predicted velocities reveal further influence of other mixed lithologies forming the sedimentary interval under analysis.

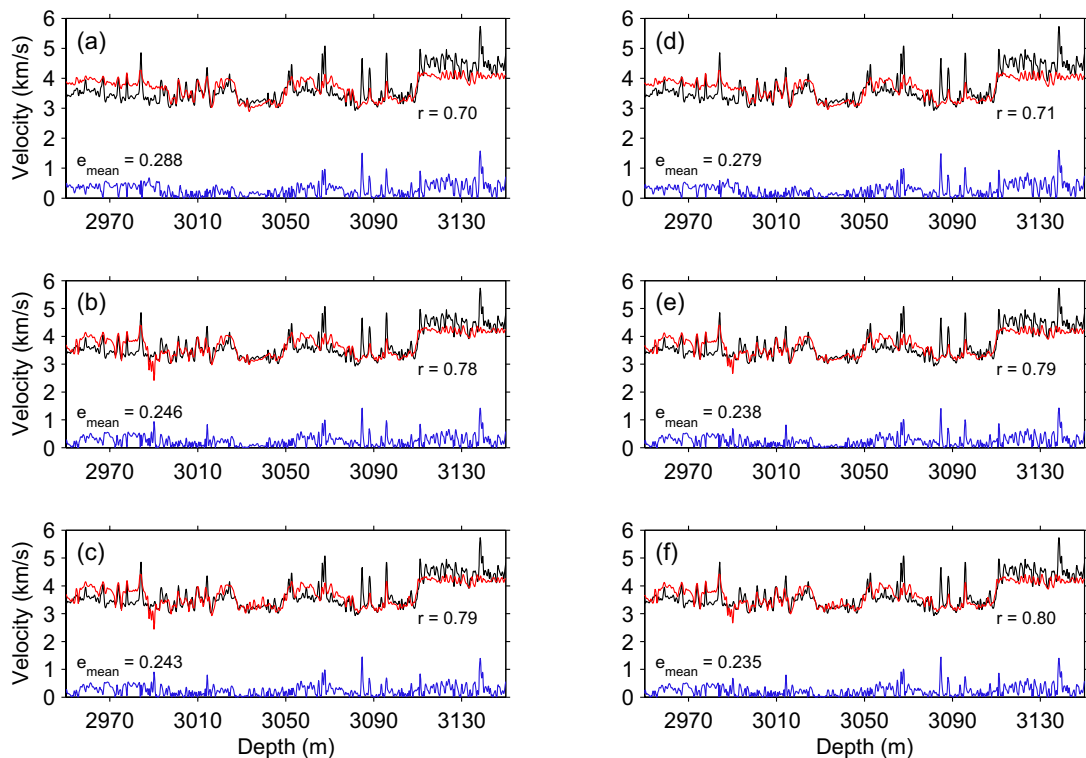


Figure 4 – Application of regression models for P-wave velocity prediction v_p^{mod} at well-4. Black curve denotes P-wave velocity v_p^{meas} converted from measured sonic log. In accordance with the regression coefficients in Table 1, the empirical models (red curves) are: (a) $v_p^{\text{mod}} = 4.27 - 4.00 \phi_e$, (b) $v_p^{\text{mod}} = 4.42 - 3.76 \phi_e - 1.44 V_{\text{clay}}$, (c) $v_p^{\text{mod}} = 4.43 - 4.06 \phi_e - 1.38 V_{\text{clay}} + 2.40 \times 10^{-3} R_{\text{ild}}$, (d) $v_p^{\text{mod}} = 4.26 \times \exp[-1.06 \phi_e]$, (e) $v_p^{\text{mod}} = 4.43 \exp[-0.99 \phi_e - 0.36 V_{\text{clay}}]$, (f) $v_p^{\text{mod}} = 4.44 \exp[-1.07 \phi_e - 0.35 V_{\text{clay}} + 5.87 \times 10^{-4} R_{\text{ild}}]$. Blue curves represent absolute residuals between measured and predicted velocity logs. Each plot correspondingly shows the mean absolute residual e_{mean} and the correlation coefficient r .

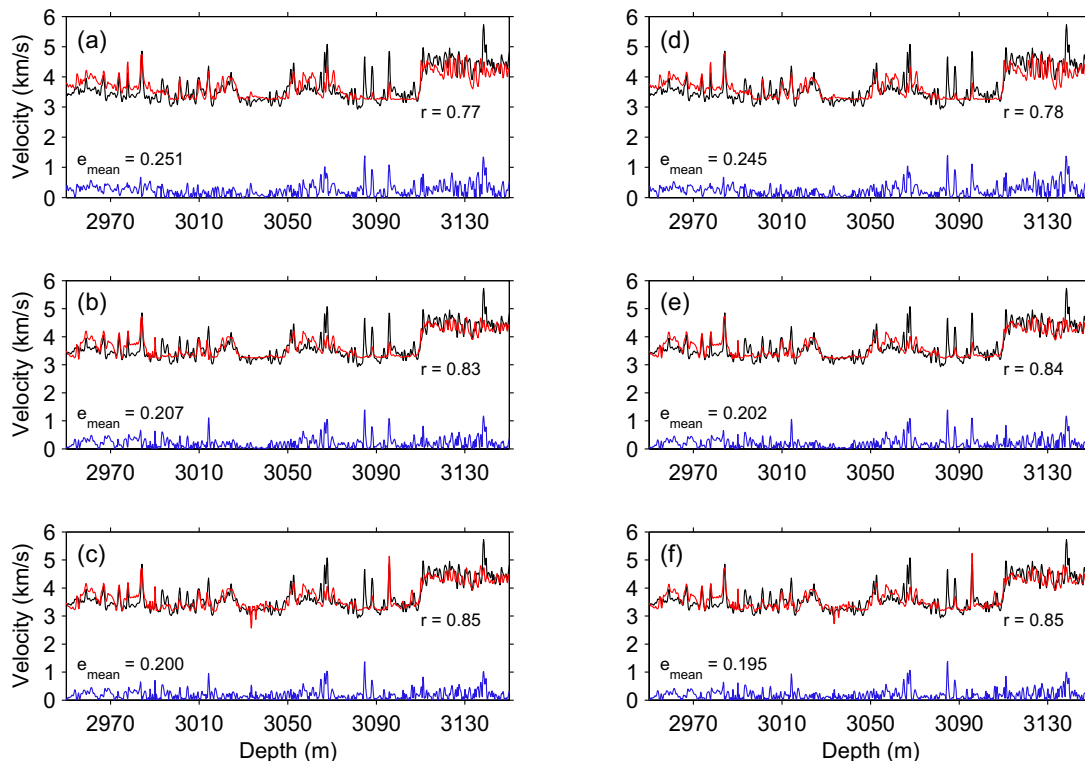


Figure 5 – Similarly as in Figure 4, but applying the following empirical models (see Table 2): (a) $v_p^{\text{mod}} = 4.74 - 12.15 \phi_e + 24.82 \phi_e^2$, (b) $v_p^{\text{mod}} = 4.80 - 8.20 \phi_e - 4.32 V_{\text{clay}} + 12.72 \phi_e V_{\text{clay}} + 10.43 (\phi_e)^2 + 2.58 (V_{\text{clay}})^2$, (c) $v_p^{\text{mod}} = 4.71 - 8.23 \phi_e - 3.91 V_{\text{clay}} + 2.14 \times 10^{-2} R_{\text{ild}} + 8.99 \phi_e V_{\text{clay}} - 5.35 \times 10^{-2} \phi_e R_{\text{ild}} - 1.18 \times 10^{-3} V_{\text{clay}} R_{\text{ild}} + 11.45 (\phi_e)^2 + 2.85 (V_{\text{clay}})^2 - 3.18 \times 10^{-5} (R_{\text{ild}})^2$, (d) $v_p^{\text{mod}} = 4.76 \exp[-2.99 \phi_e + 5.89 (\phi_e)^2]$, (e) $v_p^{\text{mod}} = 4.83 \exp[-1.95 \phi_e - 1.07 V_{\text{clay}} + 2.94 \phi_e V_{\text{clay}} + 2.21 (\phi_e)^2 + 6.48 \times 10^{-1} (V_{\text{clay}})^2]$, (f) $v_p^{\text{mod}} = 4.72 \exp[-1.94 \phi_e - 9.71 \times 10^{-1} V_{\text{clay}} + 5.31 \times 10^{-3} R_{\text{ild}} + 1.99 \phi_e V_{\text{clay}} - 1.26 \times 10^{-2} \phi_e R_{\text{ild}} - 2.32 \times 10^{-4} V_{\text{clay}} R_{\text{ild}} + 2.37 (\phi_e)^2 + 7.28 \times 10^{-1} (V_{\text{clay}})^2 - 8.85 \times 10^{-6} (R_{\text{ild}})^2]$.

In the following, we use some empirical models in order to perform comparison with the model derived by Han et al. (1986) for brine-saturated sandstone cores at 20 MPa: $v_p^{\text{mod}} = 5.49 - 6.94 \phi_e - 2.17 V_{\text{clay}}$. Although derived from saturated rock samples, this empirical model ignores fluid saturation as a parameter of velocity dependence. In Figure 8 we perform comparison using empirical models derived only from the general form in Eq. (5), for the correlation coefficients in Tables 1-4 show equivalence with the regression models obtained from Eq. (6). However, we use models in which effective porosity ϕ_e , shaliness V_{clay} and resistivity R_{ild} describe P-wave velocity dependence. In Figure 8, thicker black curves denote measured velocities converted from corresponding P-wave sonic logs.

Let us consider well-4. In Figure 8a, we plot the empirical model for v_p which can be constructed with regression coefficients in item (c) of Table 1; Figure 8b shows the v_p plot using the model with the regression coefficients in item (c) of Table 2. The calibration applying these regression models shows good predictions

of P-wave velocities in the sandstone intervals of well-4. Absolute deviations are small throughout the mixed lithologies, confirming the robustness of the 3-variable empirical models for velocity description. The regression model of Han et al. (1986) shows large misfits in the sealing intervals of well-4 because it was derived using data from brine-saturated sandstones at 20 MPa. Thus, we can infer that the sandstone intervals at this well are submitted to an effective pressure of 20 MPa.

On the other hand, Han's et al. (1986) empirical model is non-applicable to the sedimentary interval sampled in well-37. It corresponds to a clay-dominated interval resulting in a well-behaved resistivity log. The large misfits can be seen in Figures 8c and 8d. Concerning our empirical models, Figure 8c shows v_p description using the regression coefficients in item (c) of Table 3; in Figure 8d, the plotting is performed with the empirical model for v_p with regression coefficients in item (c) of Table 4. Due to the well-behaved nature of the logs at well-37, both least-squares regression models reasonably predict P-wave velocities.

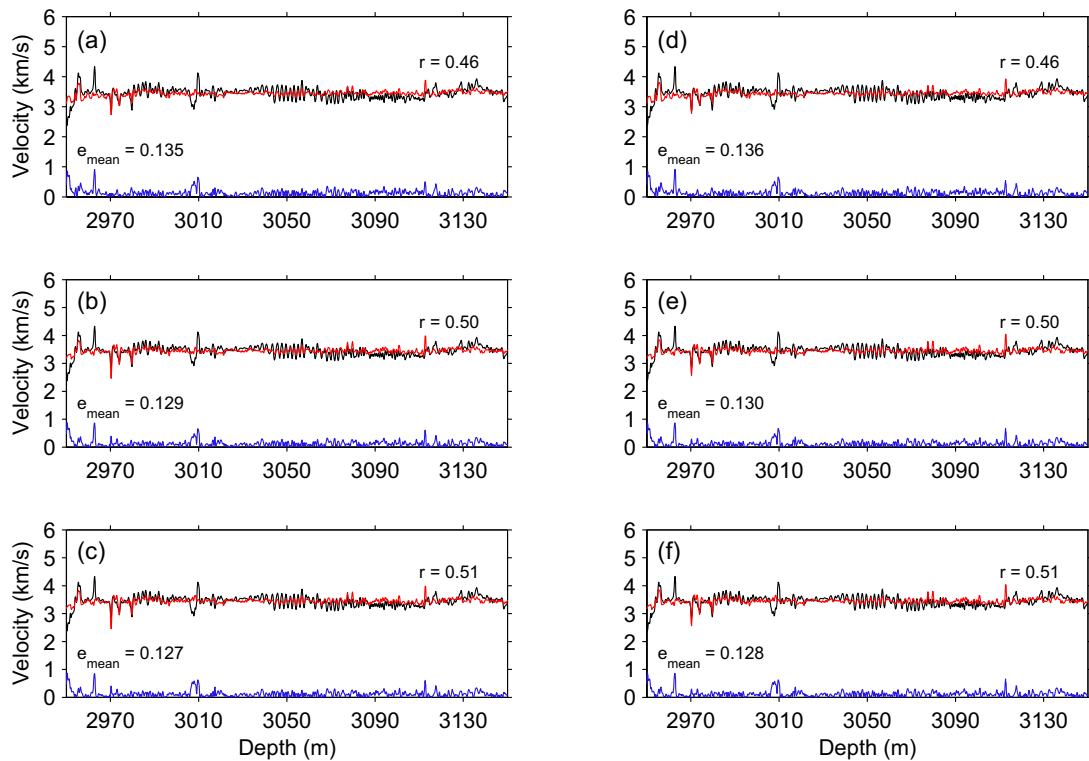


Figure 6 – Application of regression models for P-wave velocity prediction v_p^{mod} at well-37. Black curve denotes P-wave velocity v_p^{meas} converted from measured sonic log. In accordance with the regression coefficients in Table 3, the empirical models (red curves) are: (a) $v_p^{\text{mod}} = 3.88 - 3.81 \phi_e$, (b) $v_p^{\text{mod}} = 3.94 - 5.11 \phi_e + 3.88 \times 10^{-1} V_{\text{clay}}$, (c) $v_p^{\text{mod}} = 3.90 - 5.07 \phi_e + 3.89 \times 10^{-1} V_{\text{clay}} + 1.88 \times 10^{-2} R_{\text{ild}}$, (d) $v_p^{\text{mod}} = 3.92 \exp[-1.14 \phi_e]$, (e) $v_p^{\text{mod}} = 3.99 \exp[-1.53 \phi_e + 1.17 \times 10^{-1} V_{\text{clay}}]$, (f) $v_p^{\text{mod}} = 3.95 \exp[-1.52 \phi_e + 1.17 \times 10^{-1} V_{\text{clay}} + 4.96 \times 10^{-3} R_{\text{ild}}]$. Blue curves represent absolute residuals between measured and predicted velocity logs. Each plot correspondingly shows the mean absolute residual e_{mean} and the correlation coefficient r .

CONCLUSIONS

Use of regression analysis represents a very suitable procedure for establishing velocity dependence in mixed lithologies. Although most published works show core plug measurements as the main source of information, rock physical properties extracted from well log data can also be used in establishing a P-wave regression model. The importance of porosity and shaliness in describing velocity variation represents the primary choice for these parameters as the variables of the dependence. Considering resistivity as a further velocity dependence parameter may represent a refinement of the empirical model, since it can indirectly incorporate fluid-saturation effects into the velocity variation.

Additional conclusions can be drawn from the correlation coefficients in Tables 1-4. The results presented therein with 1-variable empirical models clearly exhibit the need for more information on the rock properties. For porosity as the main dependence variable, P-wave velocity can be described better than

using only shaliness or electrical resistivity. If porosity and shaliness are included in the empirical model for describing the velocity variation, the correlation coefficients increase significantly. Further incorporation of electrical resistivity as a parameter of the velocity dependence produces higher correlation coefficients. In this case, the increase in correlation coefficients is far higher for quadratic empirical models. These conclusions apply for both general forms in Eqs. (5) and (6), from which we obtained the empirical models used in the present paper.

In case of assuming water saturation S_w as an additional parameter in the velocity dependence, a preprocessing for S_w estimation will be required. However, because R_{ild} implicitly incorporates fluid saturation into the velocity dependence, assuming S_w as an additional parameter represents a redundant procedure. Moreover, improvements in the velocity predictions can be obtained by taking in the empirical models $\ln(R_{\text{ild}})$ as a parameter. In fact, use of R_{ild} in the dependence may lead to poor velocity correlations because of outliers possibly present in the electrical

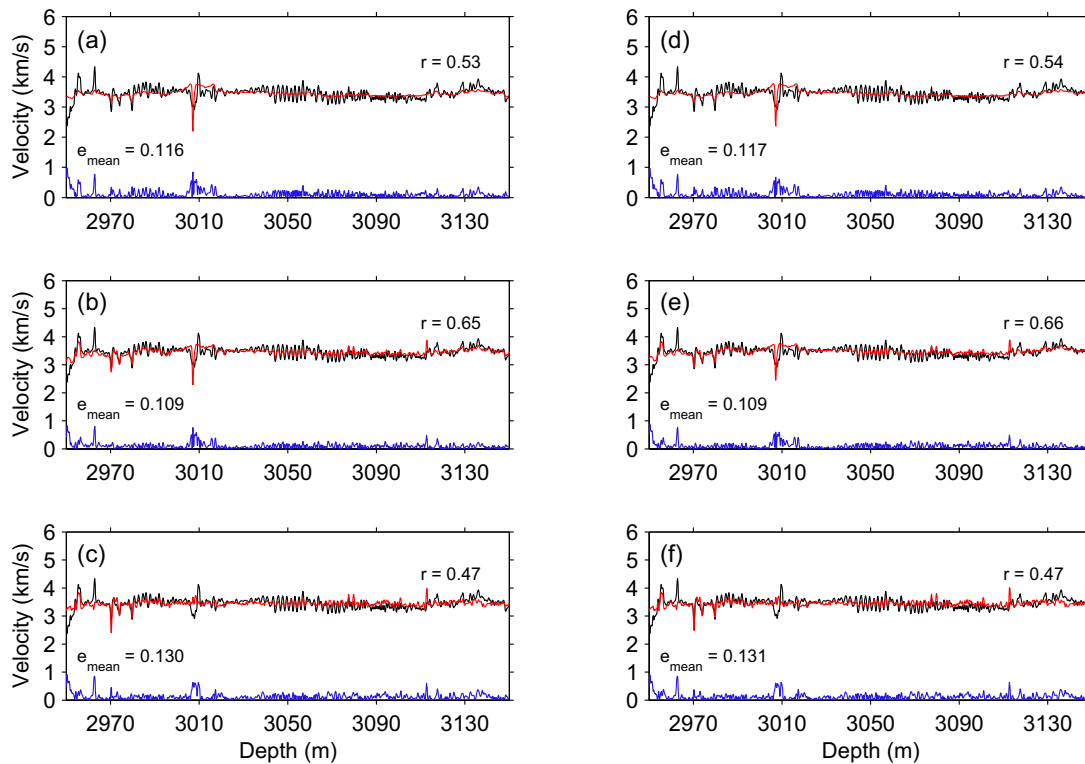


Figure 7 – Similarly as in Figure 6, but applying the following empirical models (see Table 4): (a) $v_p^{\text{mod}} = 2.92 + 3.61 \times 10^{-1} R_{\text{ild}} - 3.86 \times 10^{-2} (R_{\text{ild}})^2$, (b) $v_p^{\text{mod}} = 3.53 - 5.39 \phi_e + 2.56 \times 10^{-1} R_{\text{ild}} + 5.26 \times 10^{-1} \phi_e \times R_{\text{ild}} + 5.60 (\phi_e)^2 - 3.44 \times 10^{-2} (R_{\text{ild}})^2$, (c) $v_p^{\text{mod}} = 3.80 - 4.31 \phi_e + 5.52 \times 10^{-1} V_{\text{clay}} + 6.93 \times 10^{-2} R_{\text{ild}} + 3.10 \phi_e V_{\text{clay}} - 6.16 \times 10^{-1} \phi_e R_{\text{ild}} + 9.14 \times 10^{-3} V_{\text{clay}} R_{\text{ild}} - 2.40 (\phi_e)^2 - 8.10 \times 10^{-1} (V_{\text{clay}})^2 + 2.27 \times 10^{-3} \times (R_{\text{ild}})^2$, (d) $v_p^{\text{mod}} = 2.95 \exp[1.06 \times 10^{-1} R_{\text{ild}} - 1.14 \times 10^{-2} (R_{\text{ild}})^2]$, (e) $v_p^{\text{mod}} = 3.55 \exp[-1.57 \phi_e + 6.90 \times 10^{-2} R_{\text{ild}} + 2.02 \times 10^{-1} \phi_e R_{\text{ild}} + 1.78 (\phi_e)^2 - 1.01 \times 10^{-2} (R_{\text{ild}})^2]$, (f) $v_p^{\text{mod}} = 3.84 \exp[-1.26 \phi_e + 1.85 \times 10^{-1} V_{\text{clay}} + 1.41 \times 10^{-2} R_{\text{ild}} + 7.63 \times 10^{-1} \phi_e V_{\text{clay}} - 1.37 \times 10^{-1} \phi_e R_{\text{ild}} + 2.70 \times 10^{-3} V_{\text{clay}} R_{\text{ild}} - 1.04 (\phi_e)^2 - 2.39 \times 10^{-1} (V_{\text{clay}})^2 + 7.03 \times 10^{-4} (R_{\text{ild}})^2]$.

resistivity log. Assumption of $\ln(R_{\text{ild}})$ smooths such outliers, giving to better velocity correlations.

ACKNOWLEDGMENTS

This paper shows results of the research project “Caracterização de Anisotropia Sísmica Usando Perfis Geofísicos de Poços de Petróleo e Gás”, which has support from The National Council for Scientific and Technological Development, CNPq/Brazil (proc. no. 471647/2006-3). Preliminary results of this paper were presented at the 10th International Congress of the Brazilian Geophysical Society (SBGf), at the Rio Oil & Gas 2008 Expo and Conference and at the III Symposium of SBGf. Fabrício Augusto acknowledges a research scholarship from CAPES/Brazil for the development of his master dissertation in Geophysics at Observatório Nacional, Brazil. We sincerely appreciate the contributions of an anonymous reviewer.

REFERENCES

- ARCHIE GE. 1950. Introduction to petrophysics of reservoir rocks. Bulletin of the American Association of Petroleum Geologists, 34: 943–961.
- CASTAGNA JP, BATZLE ML & EASTWOOD RL. 1985. Relationships between compressional-wave and shear-wave velocities in clastic silicate rocks. Geophysics, 50: 571–581.
- CASTAGNA JP, BATZLE ML & KAN TK. 1993. Rock physics: The link between rock properties and AVO response. In: CASTAGNA JP & BAC-KUS MM (Eds.). Offset-dependent reflectivity – Theory and practice of AVO analysis. Investigations in Geophysics no. 8, Society of Exploration Geophysicists, OK, 135–171.
- DEWAN JT. 1983. Essentials of modern open-hole log interpretation. PennWell Books, 361 pp.
- DOMENICO SN. 1974. Effect of water saturation on seismic reflectivity of sand reservoirs encased in shale. Geophysics, 39: 759–769.

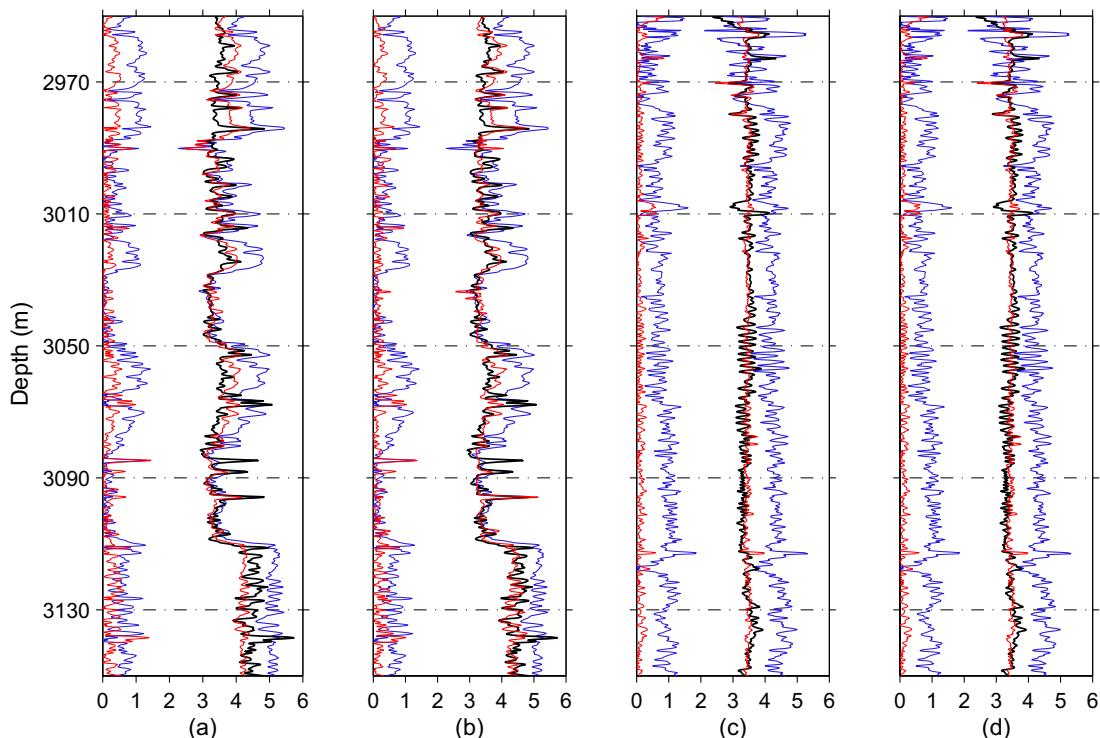


Figure 8 – Comparison of regression models for P-wave velocity prediction. The comparison is performed using the empirical relation in Han et al. (1986) for rock plugs submitted to an effective pressure of 20 MPa: $v_p^{\text{mod}} = 5.49 - 6.94 \phi_e - 2.17 V_{\text{clay}}$ (blue curve). At well-4 (red curves): (a) $v_p^{\text{mod}} = 4.43 - 4.06 \phi_e - 1.38 V_{\text{clay}} + 2.40 \times 10^{-3} R_{\text{ild}}$, and (b) $v_p^{\text{mod}} = 4.71 - 8.23 \phi_e - 3.91 V_{\text{clay}} + 2.14 \times 10^{-2} R_{\text{ild}} + 8.99 \phi_e V_{\text{clay}} - 5.35 \times 10^{-2} \phi_e R_{\text{ild}} - 1.18 \times 10^{-3} V_{\text{clay}} R_{\text{ild}} + 11.45 (\phi_e)^2 + 2.85 (V_{\text{clay}})^2 - 3.18 \times 10^{-5} (R_{\text{ild}})^2$. At well-37 (red curves): (c) $v_p^{\text{mod}} = 3.90 - 5.07 \phi_e + 3.89 \times 10^{-1} V_{\text{clay}} + 1.88 \times 10^{-2} R_{\text{ild}}$, and (d) $v_p^{\text{mod}} = 3.80 - 4.31 \phi_e + 5.52 \times 10^{-1} V_{\text{clay}} + 6.93 \times 10^{-2} R_{\text{ild}} + 3.10 \phi_e V_{\text{clay}} - 6.16 \times 10^{-1} \phi_e R_{\text{ild}} + 9.14 \times 10^{-3} V_{\text{clay}} R_{\text{ild}} - 2.40 (\phi_e)^2 - 8.10 \times 10^{-1} (V_{\text{clay}})^2 + 2.27 \times 10^{-3} (R_{\text{ild}})^2$. Absolute residuals (left curves in the plots) have the same color as the corresponding empirical model. Units in km/s.

DOMENICO SN. 1976. Effect of brine-gas mixture on velocity in an unconsolidated sand reservoir. *Geophysics*, 41: 882-894.

EBERHART-PHILLIPS D, HAN D-H & ZOBACK MD. 1989. Empirical relationships among seismic velocity, effective pressure, porosity, and clay content in sandstone. *Geophysics*, 54: 82-89.

ELLIS DV. 1987. *Well logging for Earth scientists*. Elsevier Science Publishing Co. Inc., 550 pp.

FAUST LY. 1951. Seismic velocity as a function of depth and geologic time. *Geophysics*, 16: 192-206.

FAUST LY. 1953. A velocity function including lithologic variation. *Geophysics*, 18: 271-288.

HAN D-H, NUR A & MORGAN D. 1986. Effects of porosity and clay content on wave velocities in sandstones. *Geophysics*, 51: 2093-2107.

KAUFMAN H. 1953. Velocity functions in seismic prospecting. *Geophysics*, 18: 289-297.

KLIMENTOS T. 1991. The effects of porosity-permeability-clay content on velocity of compressional waves. *Geophysics*, 56: 1930-1939.

KRIEF M, GARAT J, STELLINGWERFF J & VENTRE J. 1990. A petrophysical interpretation using the velocities of P and S waves (Full-waveform sonic). *The Log Analyst*, 31: 355-369.

LARIONOV WW. 1969. *Borehole Radiometry*. Nedra, Moscow. (In Russian). 127 pp.

LINES LR & TREITEL S. 1984. A review of least-squares inversion and its application to geophysical problems. *Geophysical Prospecting*, 32: 159-186.

MILLER SLM & STEWART RR. 1990. Effects of lithology, porosity and shaliness on P- and S-wave velocities from sonic logs. *Canadian Journal of Exploration Geophysics*, 26: 94-103.

MURPHY WF, SCHWARTZ LM & HORNBY B. 1991. Interpretation physics of Vp and Vs in sedimentary rocks. In: *Transactions of the SPWLA Thirty-Second Annual Logging Symposium*. Society of Professional Well Log Analysts, FF1-FF24.

- OLIVEIRA JK & MARTINS JL. 2003. Efeitos da porosidade e argilosi-
dade nas velocidades de ondas compressoriais no arenito Namorado,
Bacia de Campos, Brasil. In: 8th Intern. Cong. of the Brazilian Geophys.
Society, 14-18 September, Hotel Intercontinental, Rio de Janeiro, Brazil,
CD-ROM. (In Portuguese).
- PENNINGTON WD. 2001. Reservoir geophysics. *Geophysics*, 66:
25–30.
- RAYMER DS, HUNT ER & GARDNER JS. 1980. An improved sonic tran-
sit time-to-porosity transform. In: 21st Annual Meeting of the Society of
Professional Well Log Analysts, paper P.
- TIGRE CA & LUCCHESI CF. 1986. Estado atual do desenvolvimento da
Bacia de Campos e perspectivas. In: Seminário de Geologia de Desen-
volvimento e Reservatório, DEPEX-PETROBRAS, Rio de Janeiro, 1-12.
(In Portuguese).
- TOSAYA C & NUR A. 1982. Effects of diagenesis and clays on compres-
sional velocities in rocks. *Geophysical Research Letters*, 9: 5–8.
- TOKSÖZ MN, CHENG CH & TIMUR A. 1976. Velocities of seismic waves
in porous rocks. *Geophysics*, 41: 621–645.
- WATT JP, DAVIES GF & O'CONNELL RJ. 1976. The elastic properties of
composite materials. *Rev. Geophys. and Space Physics*, 14: 541–563.
- WYLLIE MRJ, GREGORY AR & GARDNER LW. 1956. Elastic wave velo-
cities in heterogeneous and porous media. *Geophysics*, 21: 41–70.
- WYLLIE MRJ, GREGORY AR & GARDNER LW. 1958. An experimental
investigation of factors affecting elastic wave velocities in porous media.
Geophysics, 23: 459–493.
- XU S & WHITE RE. 1995. A new velocity model for clay-sand mixtures.
Geophysical Prospecting, 43: 91–118.

NOTES ABOUT THE AUTHORS

Fabício de Oliveira Alves Augusto holds a BS degree (2006) in physics from Fluminense Federal University, Brazil. He earned his master dissertation (February 13th, 2009) in the post-graduation course in geophysics at Observatório Nacional, Ministry of Science and Technology, Brazil. He is a member of SBGf.

Jorge Leonardo Martins holds a BS degree (1986) in civil engineering from Veiga de Almeida University and a PhD (1992) in applied geophysics from Bahia Federal University, Brazil. He was an associate researcher at Norte Fluminense State University (1993-1998), visiting researcher at the Geophysical Institute of the Czech Acad. of Sci. (April-June/1998), post-doctoral fellow at the SW3D Consortium Project (August/1998-January/2000), visiting researcher at Campinas State University (2000), associate researcher at the Pontifical Catholic University of Rio de Janeiro (2001), and visiting professor at Rio de Janeiro State University (2002). Currently, he holds an associate researcher position at Observatório Nacional, Ministry of Science and Technology, Brazil. His professional interests include theory and practice of seismic anisotropy, azimuthal AVO analysis, integration of seismics with well log petrophysics, multicomponent seismics, and seismic data processing. He is a member of SEG and SBGf.